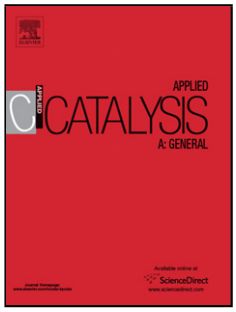

Title: Mesoporous mixed CuCo oxides as robust catalysts for liquid-phase furfural hydrogenation

Authors: Chinh Nguyen-Huy, Hojeong Lee, Jihyeon Lee, Ja Hun Kwak, Kwangjin An

PII: S0926-860X(18)30606-9
DOI: https://doi.org/10.1016/j.apcata.2018.12.010
Reference: APCATA 16914

To appear in: *Applied Catalysis A: General*

Received date: 29 July 2018
Revised date: 30 November 2018
Accepted date: 12 December 2018

Please cite this article as: Nguyen-Huy C, Lee H, Lee J, Kwak JH, An K, Mesoporous mixed CuCo oxides as robust catalysts for liquid-phase furfural hydrogenation, *Applied Catalysis A, General* (2018), https://doi.org/10.1016/j.apcata.2018.12.010

Mesoporous mixed CuCo oxides as robust catalysts for liquid-phase furfural hydrogenation

Chinh Nguyen-Huy,‡ Hojeong Lee,‡ Jihyeon Lee, Ja Hun Kwak,, and Kwangjin An**

School of Energy and Chemical Engineering, Ulsan National Institute of Science and Technology(UNIST), Ulsan 44919, Republic of Korea

‡These authors contributed equally.
*Correspondence should be addressed (E-mail: kjan@unist.ac.kr)

Graphical abstract

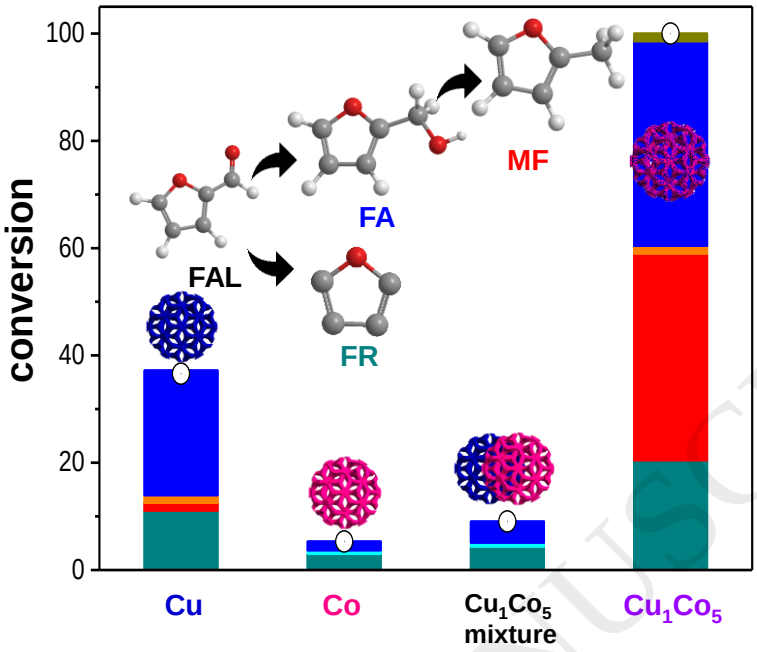

Highlights

- As-prepared mesoporous mixed CuCo oxides exhibit a high surface area and well-defined ordered mesostructure with homogenous dispersion of Cu and Co.
- Among various compositions of Cu_xCo_y (x = 1–9) studied, the Cu_1Co_5 catalyst shows the highest conversion in furfural hydrogenation, which is superior to those observed with mesoporous monometallic oxides, CuO and Co_3O_4.
- In terms of selectivity, the formation of 2-methylfuran increases with a decrease in the Cu/Co ratio in the CuCo catalyst.
- The mixed CuCo oxide catalyst is readily reduced under the reaction environment to produce metallic CuCo as the active species.
- Excellent stability and recyclability of mesoporous mixed Cu_1Co_5 oxide catalysts as well as an exceptionally high activity, surpassing those of the monometallic oxides make them promising as low-cost efficient catalysts for industrial upgradation of biomass-derived furfural.

Abstract

A series of highly ordered mesoporous CuCo oxide catalysts with a controlled composition are successfully synthesized by nanocasting from mesoporous silica, KIT-6 template. Liquid-phase furfural (FAL) hydrogenation is carried out to find the optimal composition of the CuCo oxide catalysts to achieve the best catalytic performance. As-prepared mesoporous mixed CuCo oxides exhibit a high surface area (60–135 $m^2 \cdot g^{-1}$) and a well-defined ordered mesostructure with homogenous dispersion of Cu and Co. Among various compositions of Cu_xCo_y oxides (x = 1–9) studied, the Cu_1Co_5 oxide catalyst shows the highest conversion in the

hydrogenation of FAL, which is superior to those achieved with mesoporous monometallic oxides, CuO and Co_3O_4. While 2-methylfuran is produced from furfuryl alcohol via *aldehyde hydrogenation* and subsequent *hydrogenolysis*, the formation of 2-methylfuran increased with a decrease in the Cu/Co ratio of the CuCo oxide catalyst. The mixed CuCo oxide catalyst is readily reduced under the reaction environment to produce metallic CuCo as the active species. The synergistic interactions between Cu and Co in the mixed CuCo oxide catalysts play an important role in the outstanding catalytic performance for FAL hydrogenation, which could not be achieved with either of the monometallic catalysts or their physical mixtures. The excellent stability and recyclability of mesoporous mixed CuCo oxide catalysts as well as the exceptionally high activity, surpassing those of the monometallic oxides, render them promising as a low-cost and efficient catalyst for the industrial upgrading of biomass-derived FAL.

Key words: mesoporous oxides, CuCo, furfural, hydrogenation, selectivity

1. Introduction

With the increasing demand for chemicals and fuels, it is imperative to seek and find sustainable alternatives for petroleum-based products [1]. Biomass, the only renewable source of carbon-neutral energy, can be used for the production of fuels and value-added chemicals, while addressing the need to limit the usage of declining fossil resources and related environmental issues [2,3]. Specifically, oxygen-containing chemicals are highly attractive owing to their high added value and the lower consumption of hydrogen for their production. Furfural (FAL) has been identified as one of the most important biomass-derived molecules, which are produced from hemicelluloses via acid-catalyzed hydrolysis and dehydration in a large scale [4]. Some of the important chemicals derived from FAL include furfuryl alcohol (FA), 2-methylfuran (MF), furan (FR), and tetrahydrofuran (THF). Heterogeneous catalysts are widely used for FAL conversion, owing to their higher stability and the ease of separation from the raw materials as compared to homogeneous catalysts. To date, many groups have utilized a variety of metals such as Au [5,6], Pt [7-10], Pd [11-13], Ru [14,15], Ir [16], and their alloys with a second transition metal [17-24] for FAL hydrogenation, because of their high activities. However, the high cost and scarcity of the precious metals limit their practical application. Therefore, the development of efficient catalysts based on non-precious metals is important for commercializing biomass-derived products.

Ordered mesoporous materials are widely used as catalysts as well as supports owing to their attractive properties, such as a high surface area, uniform and tunable pore size and shape, and their availability in various structures and compositions [25,26]. Moreover, mesoporous materials have a highly crystalline framework with highly uniform pores, which renders them ideal catalysts for understanding the catalytic performance related to their structure, composition, and porosity [27]. Highly ordered mesoporous transition metal oxides can be

easily prepared via the nanocasting method, in which mesoporous silica materials such as SBA-15 or KIT-6 are used as hard templates [28-32]. Owing to the versatility of the method and various structures accessible by the use various templates, mesoporous metal oxides with well-ordered pores are widely used for many catalytic studies [33-42]. However, the availability of mesoporous metal oxides, which are usually required to be reduced before using as catalysts, is very limited owing to their low structural stability under H_2-rich conditions. Often, under severe reducing conditions, the oxides are converted into metals, resulting in severe aggregation or collapse of the mesoporous framework [43]. In order to overcome this problem, mixed metal oxides might be used as alternatives, because bimetallic structures or alloys not only strengthen the material but also provide new active species which are not available in monometallic compounds [1, 44-54]. For instance, a highly stable bimetallic Cu–Co catalyst shows high activity in FAL hydrogenation, owing to the strong interaction between Cu and Co in the well-mixed oxide structure [54]. The combination of Cu metal and CoO_x is shown to be effective as a bi-metallic Cu–Co catalyst for FAL hydrogenation, since the C–O bond can be broken using the early transition metal oxides such as CoO_x, ReO_x, and MnO_x [55].

Herein, we report the synthesis of highly ordered mesoporous mixed oxides of CuCo via the nanocasting approach using cubic *Ia3d* mesoporous silica, KIT-6, as a hard-template. Catalytic properties of the mixed CuCo oxides in liquid-phase FAL hydrogenation were evaluated in comparison with those of the corresponding monometallic oxides, CuO and Co_3O_4. The catalysts were characterized via various techniques, including transmission electron microscopy (TEM), X-ray diffraction (XRD), N_2-adsorption, X-ray photoelectron spectroscopy (XPS), and temperature-programmed reduction using H_2 (H_2-TPR), to understand not only the structural and chemical properties of the mesoporous mixed CuCo oxides prepared with controlled compositions but also real active species. The catalytic activity and selectivity in the FAL

hydrogenation over various mesoporous CuCo oxide catalysts were investigated to determine the optimal composition of the catalyst. Further, distinct reaction pathways that affect the product selectivity and catalyst recyclability are also studied.

2. Experimental

2.1 Synthesis of Catalysts

2.1.1 Silica KIT-6 template

KIT-6 silica was synthesized according to a previously reported method of the cooperative assembly described elsewhere [28,31]. Briefly, 27 g of Pluronic P123 (PEO_{20}−PPO_{70}−PEO_{20}) (Sigma-Aldrich) was dissolved in a 2 L polypropylene bottle containing 980 mL of water and 43.5 mL of concentrated HCl. Then, 33.3 mL of butanol was added to the solution at 35 °C, with vigorous stirring. The mixture was stirred continuously for further 6 h. After that, 62.2 mL of tetraethoxysilane (Sigma-Aldrich) was added under vigorous stirring and the mixture was maintained at the same temperature, overnight. The hydrothermal process was then performed at 80 °C under static condition. The solid was filtered, dried overnight at 90 °C, and calcined at 550 °C for 6 h.

2.1.2 Synthesis of mesoporous oxides catalysts

Mesoporous oxides with controlled Cu and Co contents were synthesized by the nanocasting method using mesoporous silica, KIT-6, as illustrated in Scheme 1. Briefly, metal precursors, $Cu(NO_3)_2{\cdot}2.5H_2O$ and $Co(NO_3)_2{\cdot}6H_2O$ (Sigma-Aldrich), were dissolved in 6 mL water. In all cases, the concentrations of the total metal ions, Cu^{2+} and Co^{2+} + Co^{3+}, were kept constant at 4 M. In general, 6 g of KIT-6 silica was dispersed in 50 mL of toluene and the metal precursor solution was added to the mixture. After the evaporation of toluene, an ammonia solution was vaporized onto the remaining powder to catalyze the creation of an ordered oxide framework.

The ammonia-driven deposition is well-known to be an efficient method to generate a well-dispersed mesoporous Cu-based oxide. The products, mesoporous oxides with various Cu–Co compositions, were finally calcined at 300 °C for 5 h at the heating rate of 2 °C·min^{-1}. The silica templates were completely removed using 2 M aqueous NaOH solution which was pre-heated to 90 °C. The precipitates were collected by centrifugation and washed with water. After 4 cycles of washing steps with both NaOH solution and water, the mesoporous Cu–Co oxides were collected, followed by drying at 50 °C. The obtained mesoporous Cu–Co oxides are denoted as Cu_xCo_y, where, *x* and *y* represent the relative ratio of Cu and Co.

2.2. Catalysts characterization

Several physical and chemical techniques were employed to characterize the mesoporous mixed CuCo oxide catalysts. Surface properties of mesoporous materials were characterized by the Brunauer–Emmett–Teller (BET) method by nitrogen physisorption in a BEL SORP-max unit. BET specific surface area was calculated in the range of p/p_0 = 0.05–0.2. A pore diameter was calculated by the BJH method from the adsorption branches. A pore volume obtained by the BJH method. The chemical composition of the catalysts was verified by inductively coupled plasma optical emission spectroscopy (ICP-OES; Varian 700-ES). XRD patterns were recorded on a PANalytical X'Pert PRO diffractometer using Cu *Kα*radiation (λ = 0.154056 nm). The surface morphology was characterized by field-emission scanning electron microscopy (FE-SEM, Nova NanoSEM 230). Structural information was obtained by TEM (JEOL JEM-1400). High-resolution TEM (HR-TEM, JEOL JEM-2100F) and dark field and bright field images were also obtained. H_2-TPR was carried out using Auto Chem Ⅱ 2920 (Micromeritics Instruments Co., USA). X-ray photoelectric spectroscopy (XPS) analysis was carried out on a K-alpha (ThermoFisher) system equipped with an Al Kα X-ray radiation

source. In situ powder XRD data were recorded on a SmartLab (Rigaku) X-ray diffractometer equipped with a D/teX Ultra 250 detector using Cu Kαradiation (λ= 1.54184 Å).

2.3. Reaction procedure and product analysis

Mesoporous mixed CuCo oxide catalysts (10–20 mg) were taken in a 100 mL stainless-steel, high-pressure reactor containing FAL (1 g, Acros, 99%) and isopropanol (20 mL, Sigma-Aldrich). After flushing with hydrogen, the reactor was pressurized with hydrogen to 20 bar. The temperature of the reactor was then increased to 180 °C and maintained there with stirring at 600 rpm for 5 h. After the completion of the reaction, the resulting liquid product was collected and analyzed by gas chromatography (GC) using a flame ionization detector (FID; Agilent 7820A) equipped with a capillary column (DB-Wax, 30 m length, 0.32 mm internal diameter, and 0.25 μm film thickness). The following program was repeated: hold at 50 °C for 3 min, increase the temperature to 50–100 °C at the rate of 10 °C· min^{-1} and hold for 3 min, and increase the temperature to 100–200 °C at the rate of 25 °C· min^{-1} and hold for 3 min. The products, FA (Sigma-Aldrich, 98%), FR (Sigma-Aldrich, 99%), THF (Alfa Aesar, 99%), and MF (Sigma-Aldrich, 99%), were analyzed. Finally, the conversion of FAL and product selectivity were calculated as follows:

$$\text{Conversion}\ (\%) = \frac{\text{mol furfural consumed}}{\text{mol furfural fed}} \times 100$$

$$\text{Selectivity}\ (\%) = \frac{\text{mol product formed}}{\text{mol furfural consumed}} \times 100$$

3. Results and discussion

3.1. Characterization of the catalyst

Fig. 1 shows the high angle annular dark-field scanning TEM (HAADF-STEM), bright-field (BF) STEM, and HR-TEM images of mesoporous mixed Cu_xCo_y oxides. All five materials (Cu_5Co_1, Cu_3Co_1, Cu_1Co_1, Cu_1Co_3, and Cu_1Co_5 oxides) show a highly ordered pore structure (Fig. 1a–e). Upon examining many particles, the presence of the highly ordered mesoporous structure throughout the matrix is confirmed, which suggests a high level of infiltration of the template by the two precursors. Because KIT-6 has three-dimensional cubic symmetry, spherical replicas of the CuCo oxide replica were formed. Fig. 2a shows an FE-SEM image of Cu_1Co_5 oxide. Apparently, the well-ordered porous structures of Cu_1Co_5 oxide are clearly observed. HAADF-STEM, and EDS mapping images of the Cu_1Co_5 are shown in Fig. 2b–e. They reveal that the highly ordered mesoporous Cu_1Co_5 oxide contains well-mixed Cu and Co. Point scan EDS (Fig. S1) and EDS mapping (Fig. S2) analysis also confirm homogenous dispersion of Cu and Co in Cu_1Co_3 oxide.

To characterize the surface components of the mesoporous CuCo oxides, XPS was performed. Fig. 3 shows the XPS Co 2p and Cu 2p spectra of CuCo with various compositions. The binding energies of Co $2p_{3/2}$ and Co $2p_{1/2}$ are observed at 779 and 794 eV, respectively, corresponding to the characteristic spin–orbital splitting of 15.2 eV reported previously [56, 57] (Fig. 3a). After deconvolution, Co^{3+} and Co^{2+} peaks are observed at ~779.4 and 781.0 eV, respectively, which are in good agreement with the binding energies of spinel Co_3O_4 (~779.5 eV for Co^{3+} and ~780.8 eV for Co^{2+}) [41]. Satellite peaks with a relatively low intensity located between the Co $2p_{3/2}$ and Co $2p_{1/2}$ peaks indicate that Co ions are present in a partial spinel-type lattice arrangement and the Co^{3+} ions are mixed with Co^{2+} ions [58]. The asymmetric Co $2p_{1/2}$ peak confirms the existence of both Co^{2+} and Co^{3+} ions. The quantitative surface compositions in terms of Co^{2+}/Co^{3+} ratios are listed in Table 1. The surface Co^{2+}/Co^{3+} molar ratio of the mixed CuCo structures is much higher than that of Co_3O_4 (0.75) and increased with a decrease in the Cu/Co ratio (1.69 for Cu_5Co_1 and 2.41 for Cu_1Co_5). However, as the content of Co is further

increased to Cu_1Co_7 and Cu_1Co_9, the Co^{2+}/Co^{3+} ratios decreased to 2.01 and 1.84, respectively. Fig. 3b shows the XPS spectra of Cu 2p and deconvolution of the Cu $2p_{3/2}$ peaks of the mixed CuCo oxide series. Two major peaks of Cu $2p_{3/2}$ and Cu $2p_{1/2}$ are located at 933.3 and 953.1 eV, respectively. The splitting energy is 19.8 eV, which represents the formation of Cu^{2+} and the value agrees well with that reported previously [58]. The satellite peaks at the high binding energy originate from the shake-up transition due to the ligand–metal 3*d* charge transfer in the presence of Cu^{2+}. It is commonly recognized that the photoelectron peak at approximately 932.3–932.4 eV of Cu $2p_{3/2}$ is usually from tetrahedral Cu^{+}. The components at 933–934 eV with their satellites are due to octahedral Cu^{2+}. In all the mesoporous mixed CuCo oxides, tetrahedral Co^{2+} ions are dominant. These results suggest the surface structure of the CuCo to be as follows: Co^{2+} ions are partially substituted by Cu^{2+} ions in the mixed CuCo oxide structures [59, 60], while the entire structure contains well-mixed Cu and Co oxides, maintaining a homogeneous distribution of Cu and Co according to their composition.

The composition of the as-prepared mesoporous CuCo oxides was characterized by XRD (Fig. 4a). XRD patterns of monometallic oxides could be indexed to Co_3O_4 (JCPDS 42-1467) and CuO (JCPDS 45–0937). The well-resolved diffraction peaks in Fig. 4a are attributed to the high crystallinity of the resulting mesoporous oxides. Depending on the composition of Cu_xCo_y (x = 1–9), the corresponding XRD peaks are similar or intermediate between those of Co_3O_4 and CuO, indicating the successful formation of mesoporous mixed oxides, with the maintenance of the original composition of the precursors. In the XRD patterns of the oxide catalysts, no metallic species, Co, Cu, or CoCu alloy, are identified. However, the enlarged XRD patterns of the CuCo oxide catalysts (Fig. 4b) clearly show that the peaks corresponding to CuO are shifted to the positive direction, indicating an incorporation of Cu^{2+} ions into the spinel structure of Co_3O_4 with the formation of $Cu_xCo_yO_4$ compound, which is in good agreement with the XPS results. N_2

adsorption–desorption isotherms of the mesoporous CuO, Co_3O_4, and Cu_xCo_y oxides exhibit a typical type-IV characteristic with an apparent hysteresis loop at a relative pressure (p/p_0) of 0.4–0.9, indicating a well-ordered mesoporous structure with uniform pore sizes (Fig. S3). Table 1 summarizes the BET specific surface area, mean pore diameter, and pore volume of the mesoporous oxides and their relative Cu/Co ratio determined by ICP-OES. The Cu/Co ratios determined by ICP-OES match well with the actual precursor ratios used. The as-prepared mixed CuCo oxides and Co_3O_4 have high surface areas (60–135 $m^2 \cdot g^{-1}$), which are much higher than that of CuO (46 $m^2 \cdot g^{-1}$). The increase in the Co content is associated with an increase in the surface area and pore volume (Table 1). The high surface areas and pore volumes of the replicated CuCo oxides are expected to enhance their catalytic activity.

To investigate the reduction and structural evolution of the mixed CuCo oxides, H_2-TPR experiments were carried out. In general, when metal species interact with carriers, thus creating new surface compounds or altering their chemical states, the temperature at which they are reduced changes. Fig. 4c shows the TPR patterns of the Cu_xCo_y with various Cu/Co ratio (x/y = 5/1, 3/1, 1/1, 1/3, 1/5, 1/7, and 1/9) and the monometallic oxide counterparts. The H_2-TPR profile of Co_3O_4 displays two peaks at 206 and 363 °C due to hydrogen consumption. These peaks are ascribed to the two-step reduction of Co_3O_4 to Co(0), which takes place via the intermediate, CoO [61]. On the contrary, CuO shows only one peak at 275 °C, corresponding to the reduction of CuO to Cu(0) [62]. The mixed CuCo oxides show different behaviors in the H_2-TPR, depending on the ratio of Cu/Co, owing to strong interactions between Cu and Co. This characteristic indicates that the H_2-TPR proceeds through the reduction of both segregated (CuO) and mixed oxides, which has been observed in many previous studies on bimetallic CuCo catalysts [60,63,64]. Overall, the H_2-TPR profiles reveal that the main peak of the CuCo shifts to a lower temperature, as the content of Cu is increased

(Fig. 4c). Interestingly, the trend of the peak shifts in H_2-TPR correlates with the ratio of Cu/Co in the bimetallic compounds, however they are different from that of the monometallic CuO or Co_3O_4. Even with the addition of less than 10% of the counterpart element to the oxide, the characteristic peak position is appreciably changed from that of the monometallic oxide. For example, the Cu_1Co_9 oxide containing 10% Cu exhibits a strong peak at 240 °C, which is different from that of Co_3O_4 with two weak reduction peaks. The interaction between Cu and Co results in totally different reduction behavior compared to the monometallic compound.

3.2. Catalytic hydrogenation of FAL

Liquid-phase hydrogenation of FAL was carried out at 180 °C under 20 bar H_2 over mesoporous mixed CuCo oxides with controlled compositions as well as monometallic CuO and Co_3O_4 catalysts to evaluate the influence of the chemical composition of the catalysts on their catalytic activity. With the total amount of the catalysts kept the same in the FAL hydrogenation reaction, the mixed oxides of Cu_xCo_y with appropriate Cu/Co ratios show much higher FAL conversion than the monometallic oxide of CuO and Co_3O_4 (Fig. 5a). As-prepared mesoporous Co_3O_4 shows very low conversion of FAL (5.3%) with a mass activity of 0.011 mol· h^{-1}· g^{-1} (Table 2, Entry 9), and the product selectivity is toward FR and FA. This result indicates that crystalline Co_3O_4 is not an efficient catalyst for FAL hydrogenation, despite its high surface area and a well-ordered pore structure. Compared to Co_3O_4, CuO exhibits a higher activity in FAL hydrogenation (36.6% of FAL conversion), with a mass activity of 0.076 mol· h^{-1}· g^{-1} (Table 2, Entry 1). Upon introducing the co-metal in mixed oxides, the activity of the resulting mixed CuCo oxides increased further, beyond those of the monometallic oxides (Fig. 5a and Table 2). Over the Cu_1Co_5 catalyst, a full conversion (100%) was achieved with a highest mass activity of 0.208 mol· h^{-1}· g^{-1}. With a further increase in the content of Co, FAL conversions catalyzed by Cu_1Co_7 and Cu_1Co_9 catalysts obviously declined (38.3 and 18.4%, respectively). The increase in the activity of the mixed CuCo

oxide catalysts can be attributed to the hydrogen spill-over effect, whereby the aldehyde hydrogenation reaction takes place, which was also suggested by Srivastava et al [54]. Incorporation of Co as a co-metal of CuO creates well-mixed CuCo oxides owing to strong interactions between Cu and Co, as is evident from XRD, XPS and H_2-TPR analyses. In terms of the selectivity, CuO exhibits a selectivity toward FA, while the formation of MF increases with a present in the Cu/Co ratio (x/y = 5/1 to 1/5), and the Cu_1Co_5 catalyst shows the highest selectivity towards MF (62%). In order to further investigate the superior activity of the mixed oxides catalysts, control experiments were conducted with physical mixtures of mesoporous Co_3O_4 and CuO with the same Cu/Co ratios as the mixed CuCo oxides under the same reaction conditions. For all catalysts composed of physical mixtures, less than 20% FAL conversion was obtained (Fig. 5a). Fig. 5b shows selectivity of CuO, Cu_5Co_1, and Cu_1Co_5 catalysts was obtained by FAL hydrogenation reaction at the same conversion rate. As the concentration of Co increases in the mixed CuCo oxide catalysts, the selectivity toward MF is further increased. The selectivity toward MF was highest in the Cu_1Co_5 catalyst (62%). Although product selectivity varies with reaction conditions and time, high FA and MF selectivity are due to Cu and Co characteristics, respectively. On a catalyst consisting of a physical mixture of individual CuO and Co_3O_4 with controlled ratios, the surface normalized reaction rate decreases as the relative fraction of Cu decreases, indicating that the overall activity of the physically mixed catalyst is dependent on the concentration of CuO (Fig. 5c and Table 2). However, the as-prepared CuCo oxide catalyst exhibits a higher reaction rate than those of physical mixtures with the same Cu/Co ratio. In Fig. 5c, the reaction rate does not vary significantly from pure CuO to Cu_1Co_5 catalyst, and decreases to pure Co_3O_4. The overall activity of the CuCo oxide catalyst was determined by the concentration of exposed Cu. However, this value does not follow the trend of Cu/Co ratios which obtained from XPS analysis (Table 1). In addition, the different selectivity in the CuCo oxide catalyst compared to pure CuO (Fig. 5b) indicates that the activity of the CuCo oxide originated from not only the

concentration of exposed Cu but also Co. The synergistic interactions between Cu and Co within the mixed CuCo catalysts further enhanced the reaction rate in FAL hydrogenation.

3.3. Active species and reaction mechanism

To clarify the active metal species for FAL hydrogenation over mixed CuCo oxides catalysts, in situ XRD study was conducted under a flow of 100 vol.% H_2 (10 mL· min^{-1}) at 180 ºC. Fig. 6 presents time-resolved XRD patterns for CuO, Cu_5Co_1, and Cu_1Co_5 catalysts, indicating different reduction behaviors under hydrogen atmosphere at 180 ºC. The pure mesoporous CuO was converted to metallic Cu after 40 min (Fig. 6a), while the mixed Cu_5Co_1 catalyst was immediately transformed from CuO to metallic Cu (Fig. 6b). It demonstrates that the reduction of Cu_5Co_1 was faster than CuO under the same operating condition, which was consistent with H_2-TPR results. Similarly, the Co rich Cu_1Co_5 catalyst changed the structures as a function of reduction time at 180 ºC (Fig. 6c). As the time increased, the corresponding peak intensity of Co_3O_4 decreased with increasing intensity of the metallic Co, indicating that the Co_3O_4 phase was substantially reduced under hydrogen at 180 ºC. XRD patterns of spent catalysts after the reaction for 5 h are shown in Fig. 7. XRD peaks corresponding to metallic Cu and Co are observed in spent catalysts, demonstrating that the catalysts were already reduced during the reaction. In addition, we performed a blank test in the presence of isopropanol and H_2 (20 bar) over Cu_1Co_5 and Cu_5Co_1 catalysts without the addition of FAL under the same reaction conditions. The XRD patterns of the spent Cu_1Co_5 and Cu_5Co_1 catalysts (Fig. S4) demonstrate that the catalysts were already reduced by having metallic Cu and Co species during the reaction, which provided active sites for FAL hydrogenation.

The chemically and structurally combined CuCo oxide catalysts were reduced by hydrogen under the reaction conditions, which was confirmed by the highly reduced bimetallic CuCo phase as the active species. The synergistic interactions between Cu and Co within the mixed

CuCo catalysts further enhanced the reaction rate in FAL hydrogenation. It is concluded that the distinct bimetallic CuCo phase derived from the CuCo oxide catalyst plays a crucial role in their outstanding catalytic performance in the FAL hydrogenation which not be achieved with either of the monometallic catalysts or their physical mixtures.

In order to understand the specific reaction mechanism, FAL and FA hydrogenation were carried out over Cu_1Co_5 catalyst. The overall conversion of both FAL and FA, and selectivity as a function of reaction time are shown in Fig. 8. As the reaction proceeds, the FAL conversion increases with the reaction time (Fig. 8a). After 3 h, approximately 70% of FAL is converted, while the yield of FA reaches the maximum (36%), which then decreases gradually. After 9 h, FAL is completely consumed and the yields of FR and MF increased up to 27 and 60%, respectively, over the entire reaction time. These results indicate that FAL is rapidly converted to FA as a main intermediate with maximum selectivity at 3 h, and then, the yield of MF increases via hydrogenolysis at the expense of FA beyond 3 h. When FA is used as a feed over Cu_1Co_5 catalyst, a high yield in both MF and FR are observed (Fig. 8b). MF and FR production increases with increasing FA conversion. MF is mainly produced by hydrogen-assisted dehydration of FA or a dehydrogenation pathway through a methoxy intermediate [65]. FA can be directly decomposed into FR, however, alternatively and more preferably, FA is first dehydrogenated to FAL, followed by FAL decarbonylation to the FR proposed by Vorotnikov and co-workers [65]. As the FA conversion is attained to 100% shown in Fig. R3b, the FR yield also gradually increases at the expense of MF. It demonstrates a reversible reaction, in which a small fraction of MF is converted to FA again, and FA produces FR via decarbonylation. Vorotnikov et al. also concluded that FR was the only species not to form directly from MF due to the high energy for the preferred pathway [65]. In the current FA hydrogenation, after the conversion reached 100%, the FR yield is further increased, while the MF yield is

decreased, indicating that the reversed transformation of MF to FR occurs through the FA formation. A steady increase of FR over reaction time indicates that FR is not an intermediate in any of the hydrogenation/dehydrogenation reaction of FAL or FA, consistent with a previous study [65]. Based on these results, we found that there are two competitive reaction pathways for the FAL hydrogenation over the Cu_1Co_5 catalyst, as illustrated in scheme 2: *aldehyde hydrogenation* towards FA and subsequent *hydrogenolysis* to MF, and *decarbonylation* of FAL to FR.

The stability and recyclability of mixed CuCo oxide catalysts was tested by reusing both Cu_5Co_1 and Cu_1Co_5 through seven catalytic cycles. After centrifugation and washing with solvent (isopropanol), the used catalyst could be readily used in the next catalytic cycle. As shown in Fig. 9, the Cu_1Co_5 catalyst shows a full conversion of FAL in the first 2 runs and the conversion gradually decreases in the next consecutive catalytic runs up to 4 cycles, while the Cu_5Co_1 catalyst shows a steady decrease in FAL conversion. The decreased activity could be due to the deposition of organic reactants/products and/or possible carbons on the catalyst surface during the reaction. To remove the possible deposits, the catalysts were dried at 100 °C, followed by calcination in air at 300 °C for 2 h. By this step, the potentially adsorbed or deposited organic/carbon species were removed without catalyst collapse. As expected, the catalyst could be regenerated after the 4th cycle, and the conversion of FAL was recovered, since the organic molecules deposited were burned during the calcination and the surface active sites of the catalyst were recovered from the coke.

4. Conclusion

We developed a series of highly ordered mesoporous mixed CuCo oxide catalysts via the nanocasting approach using silica templates. The prepared CuCo replicas possess high surface areas, which are higher than that of mesoporous CuO. For the liquid-phase hydrogenation of

FAL, the optimized Cu_1Co_5 catalyst shows the best catalytic performance (100 % FAL conversion) in comparison with the mesoporous monometallic oxides, CuO and Co_3O_4. The FAL hydrogenation over mixed CuCo oxide catalysts follows two reaction pathways: *aldehyde hydrogenation* toward FA and then *hydrogenolysis* to MF, and *decarbonylation* toward FR. The formation of MF increased with a decrease in the Cu/Co ratio. Physical mixtures of mesoporous Co_3O_4 and CuO with the same Cu/Co ratios as the mixed CuCo oxides showed much less activity than the mixed oxides catalysts under the same reaction conditions. The chemically and structurally combined CuCo oxide catalysts were reduced by hydrogen under the reaction conditions, by producing the highly reduced bimetallic CuCo phase as the active species. Combined results reveal that the synergistic interaction between Cu and Co in the mixed CuCo catalysts plays a crucial role in the outstanding catalytic performance in the FAL hydrogenation. Moreover, the recovered mixed CuCo catalyst shows good regenerability during consecutive catalytic runs. The efficient and versatile mixed CuCo oxides are not only promising catalysts for effectively upgrading biomass-derived FAL, but also provide a useful guidance for the rational design of low-cost catalysts without using precious metals.

ACKNOWLEDGEMENTS: This research was supported by Basic Science Research Program (2018R1A1A1A05079555) and Technology Development Program to Solve Climate Changes (2017M1A2A2087630) of the National Research Foundation of Korea (NRF) funded by the Ministry of Science and ICT, and MOTIE(KIAT_N0001754).

References

[1] D.M. Alonso, S.G. Wettstein, J.A. Dumesic, Chem. Soc. Rev. 41 (2012) 8075-8098.
[2] J.C. Serrano-Ruiz, J.A. Dumesic, Energ. Environ. Sci. 4 (2011) 83-99.
[3] Y.C. Shi, E.H. Xing, K.J. Wu, J.L. Wang, M.D. Yang, Y.L. Wu, Catal. Sci. Technol. 7 (2017) 2385-2415.
[4] J.P. Lange, E. van der Heide, J. van Buijtenen, R. Price, Chemsuschem 5 (2012) 150-166.
[5] M.S. Li, L. Collado, F. Cardenas-Lizana, M.A. Keane, Catal. Lett. 148 (2018) 90-96.
[6] S.H. Zhu, Y.F. Xue, J. Guo, Y.L. Cen, J.G. Wang, W.B. Fan, Acs Catal. 6 (2016) 2035-2042.
[7] M.J. Taylor, L. Jiang, J. Reichert, A.C. Papageorgiou, S.K. Beaumont, K. Wilson, A.F. Lee, J.V. Barth, G. Kyriakou, J. Phys. Chem. C 121 (2017) 8490-8497.
[8] J. Kijenski, P. Winiarek, T. Paryjczak, A. Lewicki, A. Mikolajska, Appl. Catal. a-Gen. 233 (2002) 171-182.
[9] K. An, N. Musselwhite, G. Kennedy, V.V. Pushkarev, L.R. Baker, G.A. Somorjai, J. Colloid Interf. Sci. 392 (2013) 122-128.
[10] V.V. Pushkarev, N. Musselwhite, K.J. An, S. Alayoglu, G.A. Somorjai, Nano Lett. 12 (2012) 5196-5201.
[11] S.M. Rogers, C.R.A. Catlow, C.E. Chan-Thaw, A. Chutia, N. Jian, R.E. Palmer, M. Perdjon, A. Thetford, N. Dimitratos, A. Villa, P.P. Wells, Acs Catal. 7 (2017) 2266-2274.
[12] C.T. Wang, L. Wang, J. Zhang, H. Wang, J.P. Lewis, F.S. Xiao, J. Am. Chem. Soc. 138 (2016) 7880-7883.
[13] C. Nguyen-Huy, J.S. Kim, S. Yoon, E. Yang, J.H. Kwak, M.S. Lee, K. An, Fuel 226 (2018) 607-617.
[14] P. Panagiotopoulou, D.G. Vlachos, Appl. Catal. a-Gen. 480 (2014) 17-24.
[15] J. Jae, W.Q. Zheng, R.F. Lobo, D.G. Vlachos, Chemsuschem 6 (2013) 1158-1162.
[16] N.S. Date, A.M. Hengne, K.W. Huang, R.C. Chikate, C.V. Rode, Green Chem. 20 (2018) 2027-2037.
[17] A.B. Merlo, V. Vetere, J.F. Ruggera, M.L. Casella, Catal. Commun. 10 (2009) 1665-1669.
[18] M.G. Dohade, P.L. Dhepe, Green Chem. 19 (2017) 1144-1154.
[19] S. Sitthisa, T. Pham, T. Prasomsri, T. Sooknoi, R.G. Mallinson, D.E. Resasco, J. Catal. 280 (2011) 17-27.
[20] N. Pino, S. Sitthisa, Q.H. Tan, T. Souza, D. Lopez, D.E. Resasco, J. Catal. 350 (2017) 30-40.
[21] K. Fulajtarova, T. Sotak, M. Hronec, I. Vavra, E. Dobrocka, M. Omastova, Appl. Catal. a-Gen. 502 (2015) 78-85.
[22] M. Hronec, K. Fulajtarova, I. Vavra, T. Sotak, E. Dobrocka, M. Micusik, Appl. Catal. B-Environ. 181 (2016) 210-219.
[23] X. Chang, A.F. Liu, B. Cai, J.Y. Luo, H. Pan, Y.B. Huang, Chemsuschem 9 (2016) 3330-3337.
[24] Y. Nakagawa, K. Takada, M. Tamura, K. Tomishige, Acs Catal. 4 (2014) 2718-2726.
[25] A. Corma, Chem. Rev. 97 (1997) 2373-2419.
[26] Y. Wan, D.Y. Zhao, Chem. Rev. 107 (2007) 2821-2860.
[27] P. Bhanja, A. Bhaumik, Fuel 185 (2016) 432-441.
[28] A.H. Lu, F. Schuth, Adv. Mater. 18 (2006) 1793-1805.
[29] A. Stein, B.E. Wilson, S.G. Rudisill, Chem. Soc. Rev. 42 (2013) 2763-2803.

[30] S.H. Joo, S.J. Choi, I. Oh, J. Kwak, Z. Liu, O. Terasaki, R. Ryoo, Nature 414 (2001) 470-470.
[31] X.H. Deng, K. Chen, H. Tuysuz, Chem. Mater. 29 (2017) 40-52.
[32] F. Jiao, J.C. Jumas, M. Womes, A.V. Chadwick, A. Harrison, P.G. Bruce, J. Am. Chem. Soc. 128 (2006) 12905-12909.
[33] W.B. Yue, A.H. Hill, A. Harrison, W.Z. Zhou, Chem. Commun. (2007) 2518-2520.
[34] H. Tuysuz, Y. Liu, C. Weidenthaler, F. Schuth, J. Am. Chem. Soc. 130 (2008) 14108-14110.
[35] D. Gu, C.J. Jia, C. Weidenthaler, H.J. Bongard, B. Spliethoff, W. Schmidt, F. Schuth, J. Am. Chem. Soc. 137 (2015) 11407-11418.
[36] C.Y. Ma, Z. Mu, J.J. Li, Y.G. Jin, J. Cheng, G.Q. Lu, Z.P. Hao, S.Z. Qiao, J. Am. Chem. Soc. 132 (2010) 2608-2613.
[37] Y. Ren, Z. Ma, P.G. Bruce, Chem. Soc. Rev. 41 (2012) 4909-4927.
[38] X. He, D. Antonelli, Angew Chem. Int. Edit. 41 (2002) 214-229.
[39] J.S. Hu, L.S. Zhong, W.G. Song, L.J. Wan, Adv. Mater. 20 (2008) 2977-2982.
[40] S.J. Sun, Q.M. Gao, H.L. Wang, J.K. Zhu, H.L. Guo, Appl. Catal. B-Environ. 97 (2010) 284-291.
[41] B.Y. Bai, H. Arandiyan, J.H. Li, Appl. Catal. B-Environ. 142 (2013) 677-683.
[42] A. Taguchi, F. Schuth, Micropor. Mesopor. Mat. 77 (2005) 1-45.
[43] C.I. Ahn, H.M. Koo, J.M. Jo, H.S. Roh, J.B. Lee, Y.J. Lee, E.J. Jang, J.W. Bae, Appl. Catal. B-Environ. 180 (2016) 139-149.
[44] C.Z. Yuan, H.B. Wu, Y. Xie, X.W. Lou, Angew Chem. Int. Edit. 53 (2014) 1488-1504.
[45] M.M. Bettahar, G. Costentin, L. Savary, J.C. Lavalley, Appl. Catal. a-Gen. 145 (1996) 1-48.
[46] D.P. Debecker, V. Hulea, P.H. Mutin, Appl. Catal. a-Gen. 451 (2013) 192-206.
[47] T.P. Sulmonetti, S.H. Pang, M.T. Claure, S. Lee, D.A. Cullen, P.K. Agrawal, C.W. Jones, Appl. Catal. a-Gen. 517 (2016) 187-195.
[48] K.L. Deutsch, B.H. Shanks, Appl. Catal. a-Gen. 470 (2014) 390-397.
[49] C. Shi, Y. Wang, A.M. Zhu, B.B. Chen, C. Au, Catal. Commun. 28 (2012) 18-22.
[50] Y. Wang, A.M. Zhu, B.B. Chen, M. Crocker, C. Shi, Catal. Commun. 36 (2013) 52-57.
[51] J. Wu, G. Gao, J.L. Li, P. Sun, X.D. Long, F.W. Li, Appl. Catal. B-Environ. 203 (2017) 227-236.
[52] Z.Y. Tian, H. Vieker, P.M. Kouotou, A. Beyer, Faraday Discuss 177 (2015) 249-262.
[53] M. Sankar, N. Dimitratos, P.J. Miedziak, P.P. Wells, C.J. Kiely, G.J. Hutchings, Chem. Soc. Rev. 41 (2012) 8099-8139.
[54] S. Srivastava, G.C. Jadeja, J. Parikh, Rsc Adv. 6 (2016) 1649-1658.
[55] W.J. Xu, H.F. Wang, X.H. Liu, J.W. Ren, Y.Q. Wang, G.Z. Lu, Chem. Commun. 47 (2011) 3924-3926.
[56] W.F. Wei, W.X. Chen, D.G. Ivey, Chem. Mater. 20 (2008) 1941-1947.
[57] D. Barreca, C. Massignan, S. Daolio, M. Fabrizio, C. Piccirillo, L. Armelao, E. Tondello, Chem. Mater. 13 (2001) 588-593.
[58] A. Amri, Z.T. Jiang, X.L. Zhao, Z.H. Xie, C.Y. Yin, N. Ali, N. Mondinos, M.M. Rahman, D. Habibi, Surf. Coat. Tech. 239 (2014) 212-221.
[59] M. De Koninck, S.C. Poirier, B. Marsan, J. Electrochem. Soc. 153 (2006) A2103-A2110.
[60] G. Fierro, M. Lo Jacono, M. Inversi, R. Dragone, P. Porta, Top. Catal. 10 (2000) 39-48.

[61] Y.X. Liu, H.X. Dai, J.G. Deng, S.H. Xie, H.G. Yang, W. Tan, W. Han, Y. Jiang, G.S. Guo, J. Catal. 309 (2014) 408-418.
[62] M.F. Luo, Y.J. Zhong, X.X. Yuan, X.M. Zheng, Appl. Catal. a-Gen. 162 (1997) 121-131.
[63] A.J. Marchi, J.I. Dicosimo, C.R. Apesteguia, Catal. Today 15 (1992) 383-394.
[64] D.V. Cesar, C.A. Perez, V.M.M. Salim, M. Schmal, Appl. Catal. a-Gen. 176 (1999) 205-212.
[65] V. Vorotnikov, G. Mpourmpakis, D.G. Vlachos, Acs Catal. 2 (2012) 2496-2504.

Table 1. Results of nitrogen adsorption-desorption, ICP-OES, and XPS analyses of CuCo oxides.

Catalyst	Nitrogen adsorption-desorption			ICP-OES		XPS	
	Surface area (S_{BET}), ($m^2 \cdot g^{-1}$)	Pore size (BJH), (nm)	Total pore volume ($cm^3 \cdot g^{-1}$)	Cu/Co	Theoretical	Cu/Co	Co^{2+}/Co^{3+}
CuO	46	8	0.09	-	-	-	-
Cu_5Co_1	60	16	0.24	4.72	5	1.64	1.69
Cu_3Co_1	94	14	0.34	2.90	3	1.79	1.71
Cu_1Co_1	129	17	0.54	0.89	1	1.02	1.72
Cu_1Co_3	135	18	0.59	0.35	0.33	0.48	2.27
Cu_1Co_5	117	12	0.35	0.18	0.2	0.21	2.41
Cu_1Co_7	120	19	0.58	0.13	0.13	0.15	2.01
Cu_1Co_9	119	15	0.45	0.11	0.1	0.15	1.84
Co_3O_4	124	15	0.48	-	-	-	0.75

Table 2. Results of catalytic hydrogenation of FAL over mesoporous CuCo oxides [a]

Entry	Catalyst	Conversion (%)	Mass reaction rate [mol· h^{-1}· g^{-1}]	Area reaction rate [mol· h^{-1}· m^{-2}]	Yield (%)				
					FR	MF	FA	Cyclo-pentanol	Other
1	CuO	36.6	0.076	1.65	11.1	1.4	23.3	1.4	-
2	Cu_5Co_1	37.4	0.078	1.30	10.1	5.2	20.0	2.0	-
3	Cu_3Co_1	62.9	0.131	1.39	19.0	7.2	34.3	2.4	-
4	Cu_1Co_1	82.5	0.172	1.33	26.1	16.5	37.3	2.5	-
5	Cu_1Co_3	87.5	0.182	1.35	27.6	19.8	37.6	2.4	-
6	Cu_1Co_5	100	0.208	1.78	20.5	38.5	38.1	1.5	1.4
7	Cu_1Co_7	38.3	0.079	0.66	9.5	4.6	24.2	-	-
8	Cu_1Co_9	18.4	0.038	0.32	4.5	1.9	12.1	-	-
9	Co_3O_4	5.3	0.011	0.09	3.0	-	1.6	-	-

[a] Reaction conditions: FAL: 1 g, isopropanol: 20 mL, catalyst: 10 mg, H_2: 20 bar, reaction temperature: 180 °C, reaction time: 5 h, stirring speed: 600 rpm.

List of Figure

Fig. 1. (a–e) HAADF-STEM, (f–j) BF-STEM, and (k–o) HR-TEM of mesoporous Cu_xCo_y oxides: (a,f,k) Cu_5Co_1, (b,g,i) Cu_3Co_1, (c,h,m) Cu_1Co_1, (d,i,n) Cu_1Co_3, and (e,j,o) Cu_1Co_5. Insets show illustrations of mesoporous Cu_xCo_y: Co in pink and Cu in blue.

Fig. 2. (a) SEM and (b) HAADF-STEM images of mesoporous Cu_1Co_5 oxides. (c–e) EDS mapping performed at an acceleration voltage of 200 kV: O (K line) in red, Cu (K line) in blue, and Co (K line) in pink.

Fig. 3. (a) Co 2p and (b) Cu 2p XPS spectra of mesoporous CuCo oxides.

Fig. 4. (a) XRD patterns and (b) their enlarged areas of mesoporous CuCo oxides with different composition.

Fig. 5. (a) FAL conversion and selectivity as a function of reaction time over mesoporous CuCo catalysts with controlled composition (* indicates a catalyst consisting of a physical mixture of individual CuO and Co_3O_4 mixed at a controlled rate). (b) FAL conversion and selectivity after the 10 h reaction over CuO, Cu_5Co_1, and Cu_1Co_5 catalysts. (c) Surface normalized reaction rate. Reaction conditions: FA (1 g), isopropanol (20 mL), catalyst (10 mg), H_2 (20 bar), reaction temperature (180 °C), stirring speed (600 rpm).

Fig. 6. In situ XRD patterns of (a) CuO, (b) Cu_5Co_1, and (c) Cu_1Co_5 under hydrogen atmosphere at 180 ºC.

Fig. 7. XRD patterns and enlarged XRD patterns of fresh and spent catalyst: (a,c) Cu_1Co_5, (b,d) Cu_5Co_1.

Fig. 8. (a) FAL and (b) FA conversion and selectivity as a function of reaction time over mixed Cu_1Co_5 oxide catalyst. Reaction conditions: FAL or FA (1 g), isopropanol (20 mL), catalyst (10 mg), H_2 (20 bar), reaction temperature (180 °C), stirring speed (600 rpm).

Fig. 9. Recycling test for FAL conversion over Cu_1Co_5 and Cu_5Co_1 catalysts. (* indicates that the catalyst was reactivated by calcination in air flow at 300 °C for 2 h). Reaction conditions: FAL (1 g), isopropanol (20 mL), catalyst (20 mg), H_2 (20 bar), reaction temperature (180 °C), stirring speed (600 rpm).

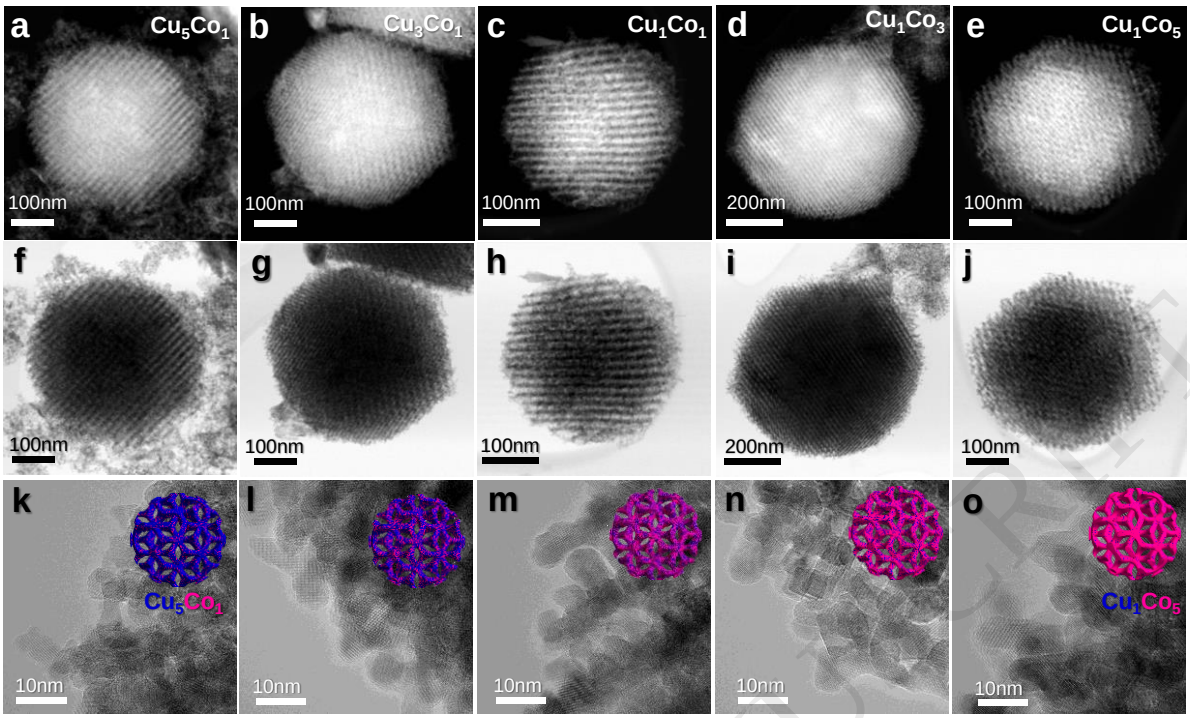

Fig. 1.

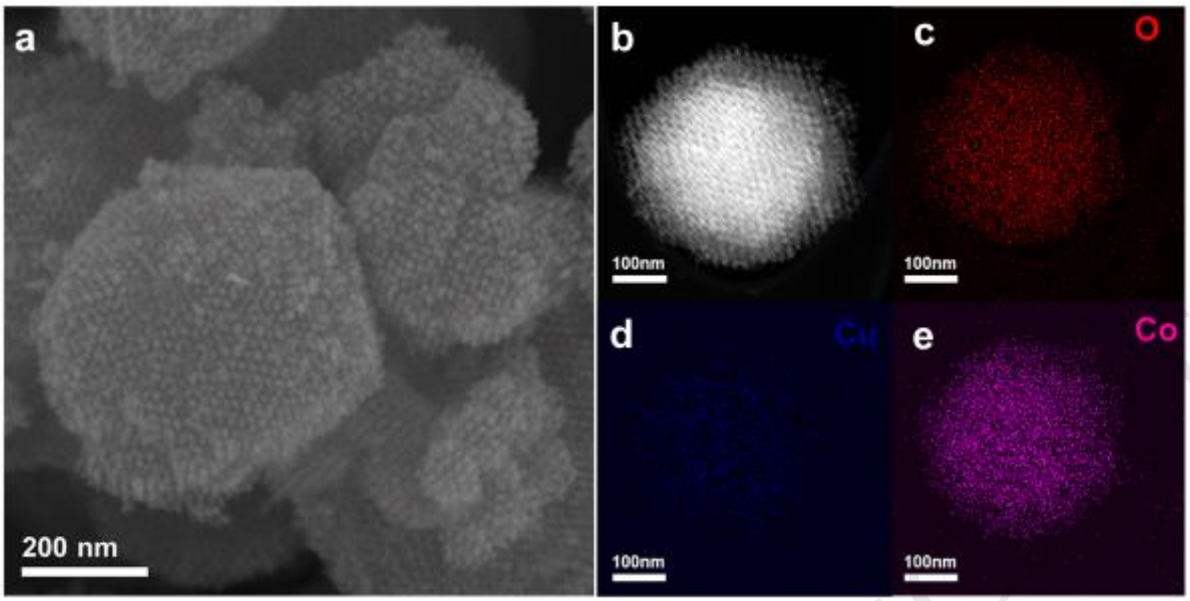

Fig. 2.

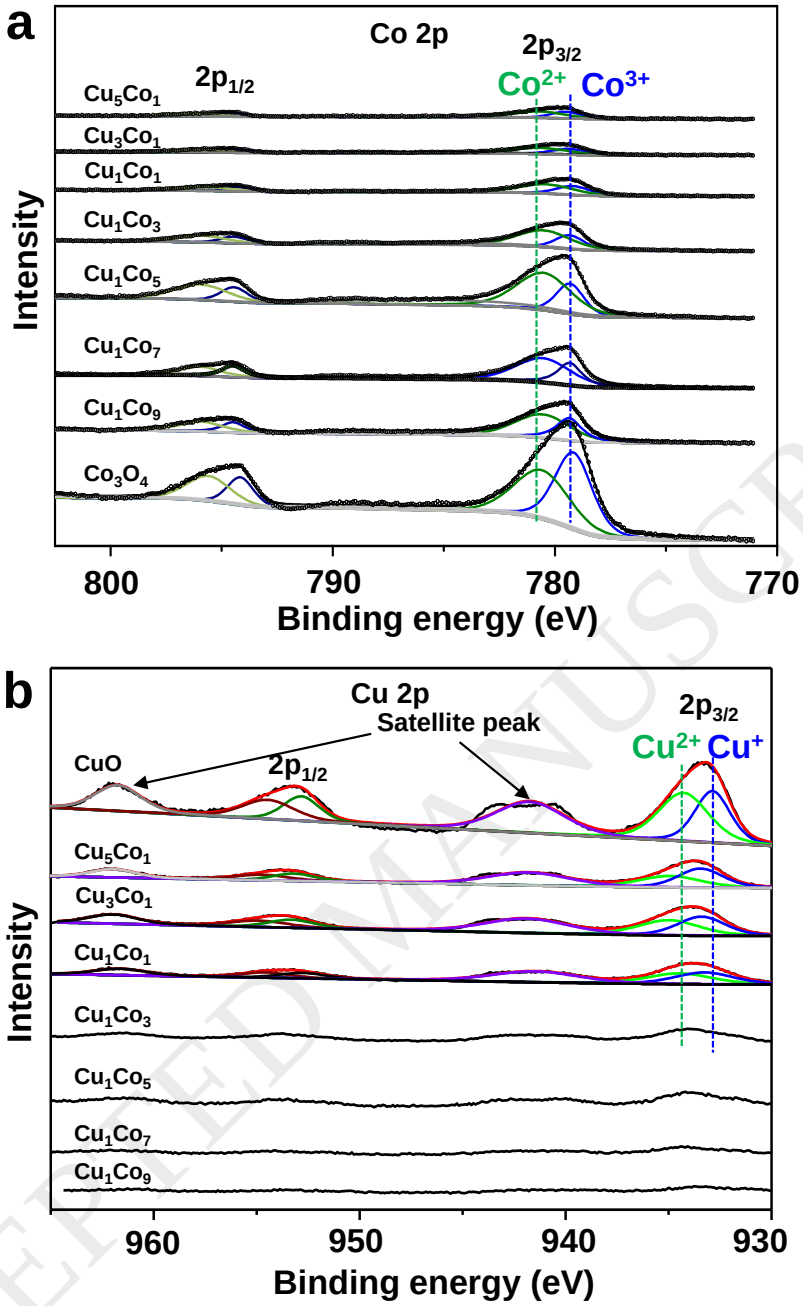

Fig. 3.

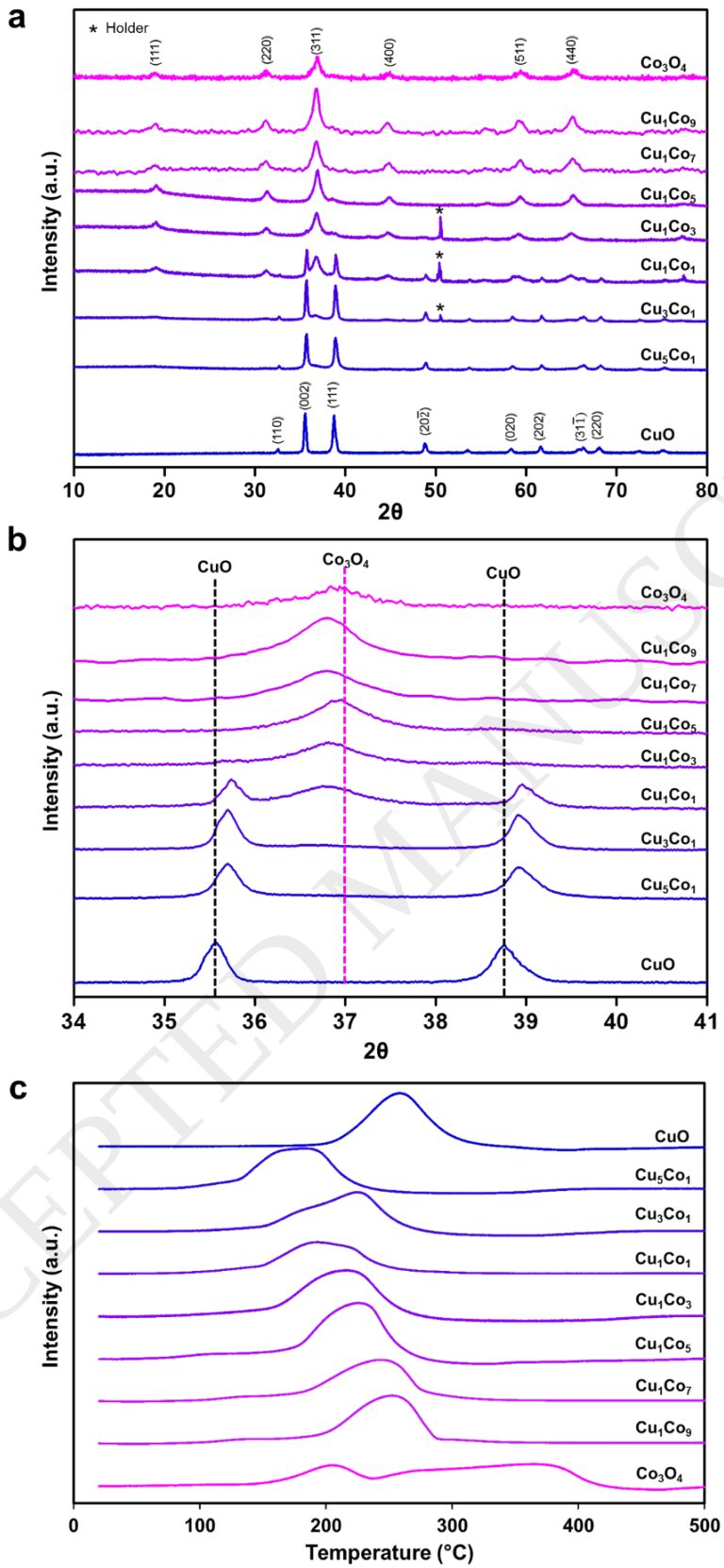

Fig. 4.

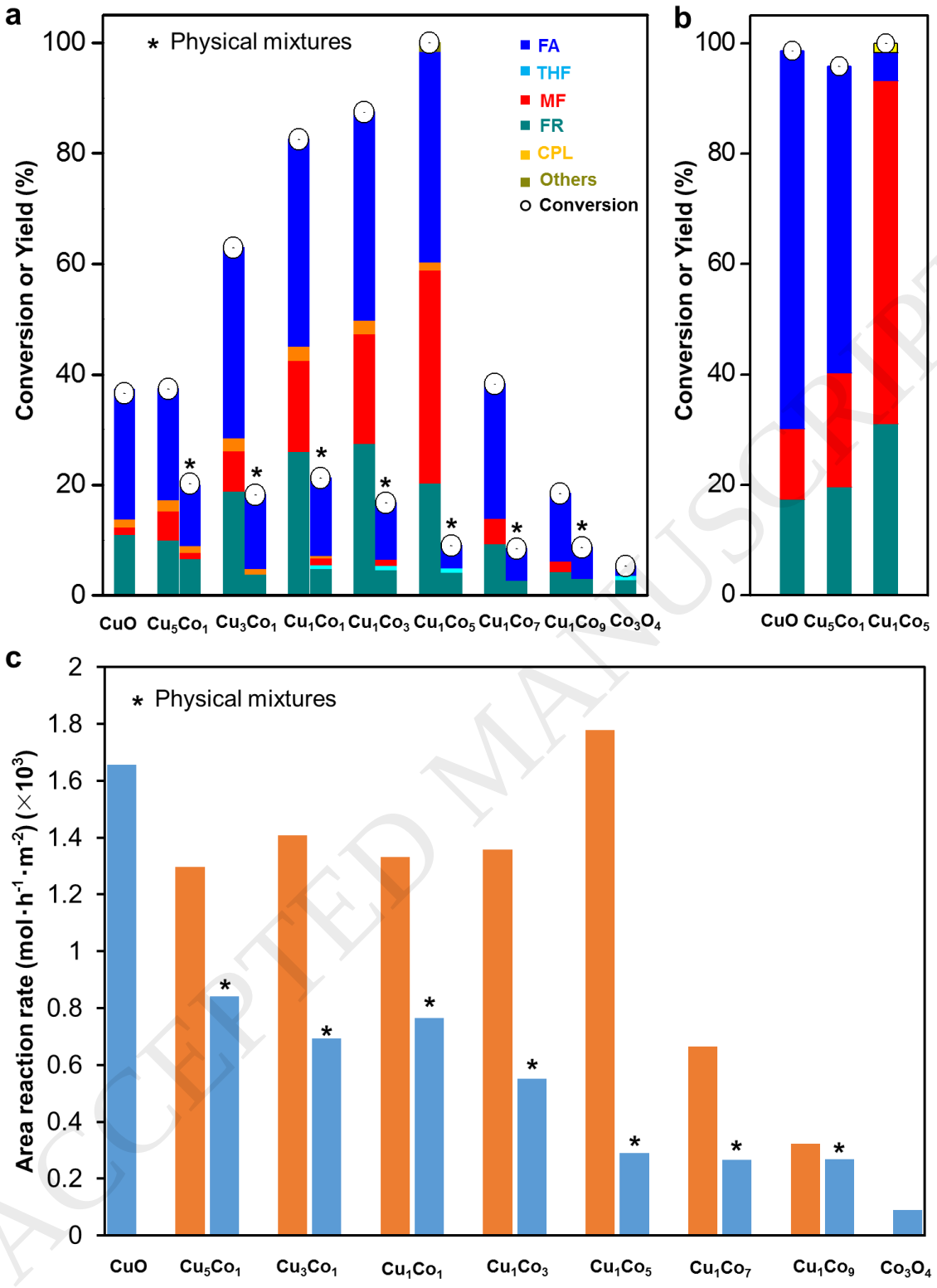

Fig. 5.

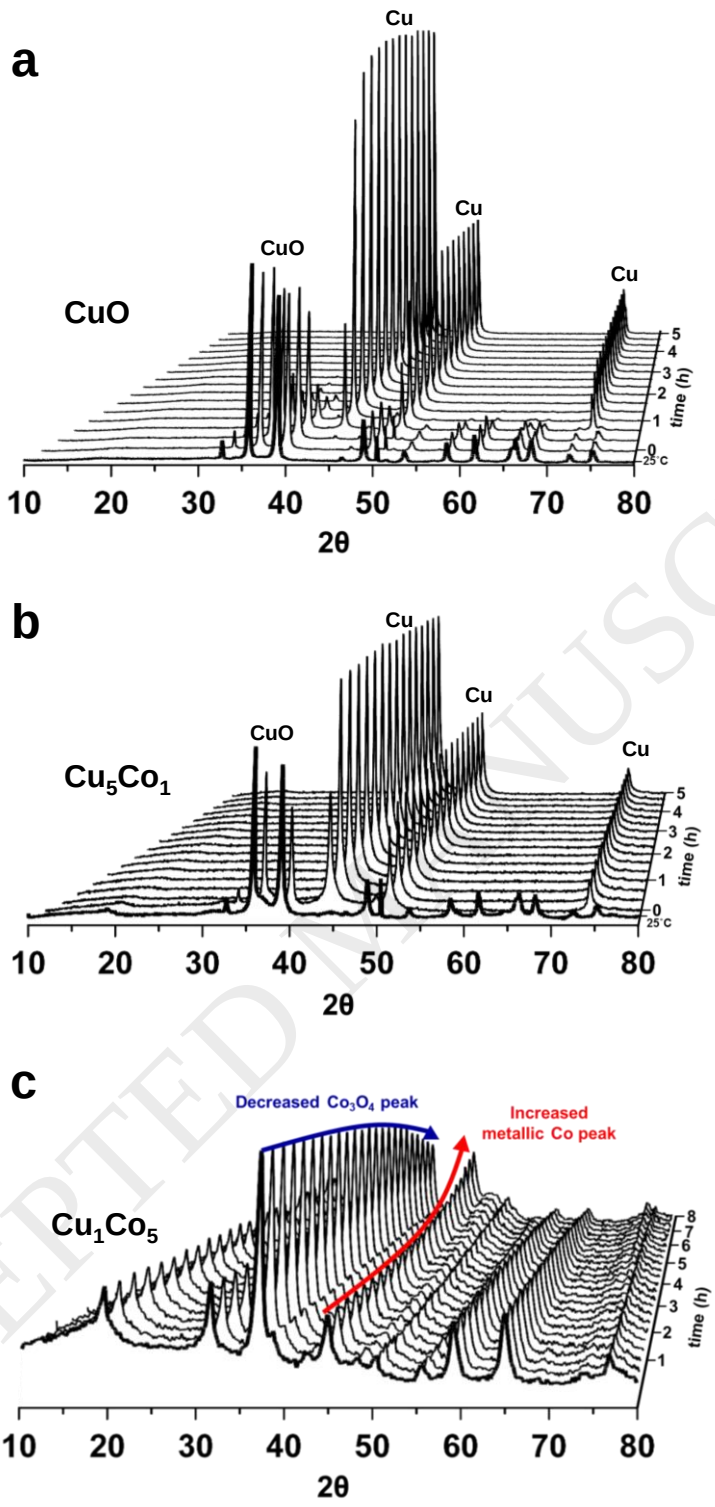

Fig. 6.

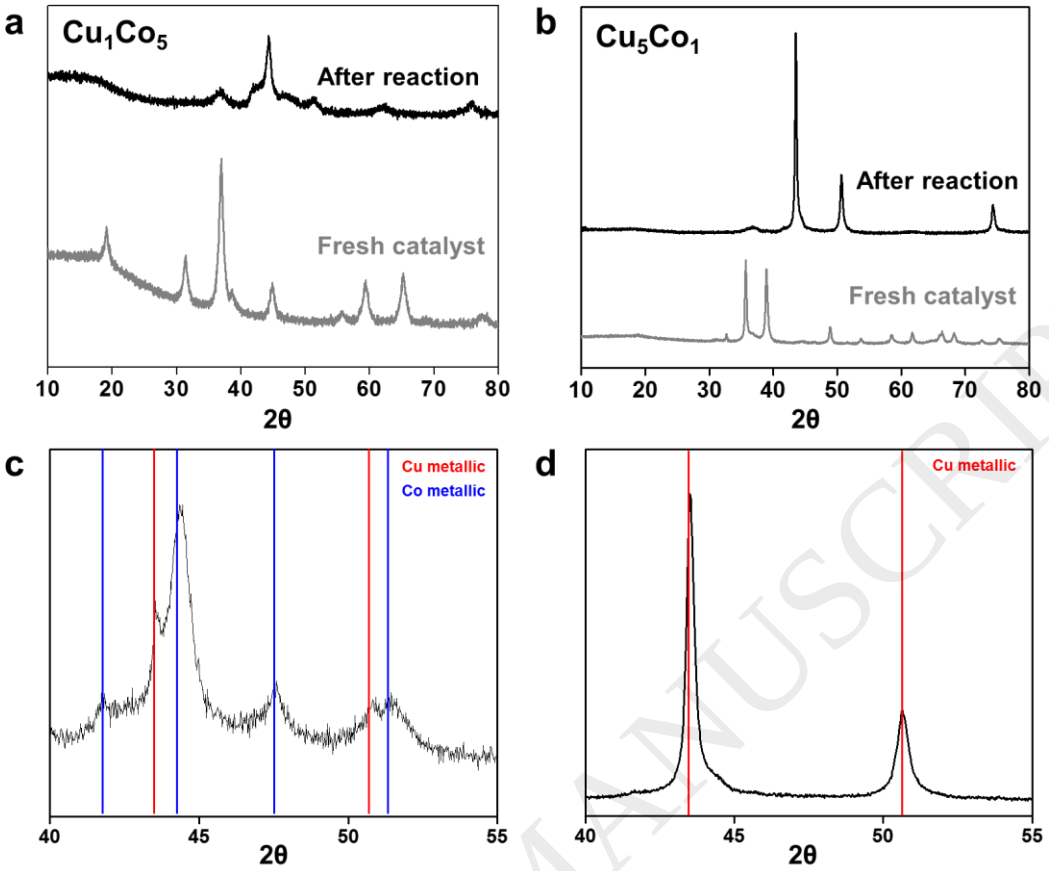

Fig. 7.

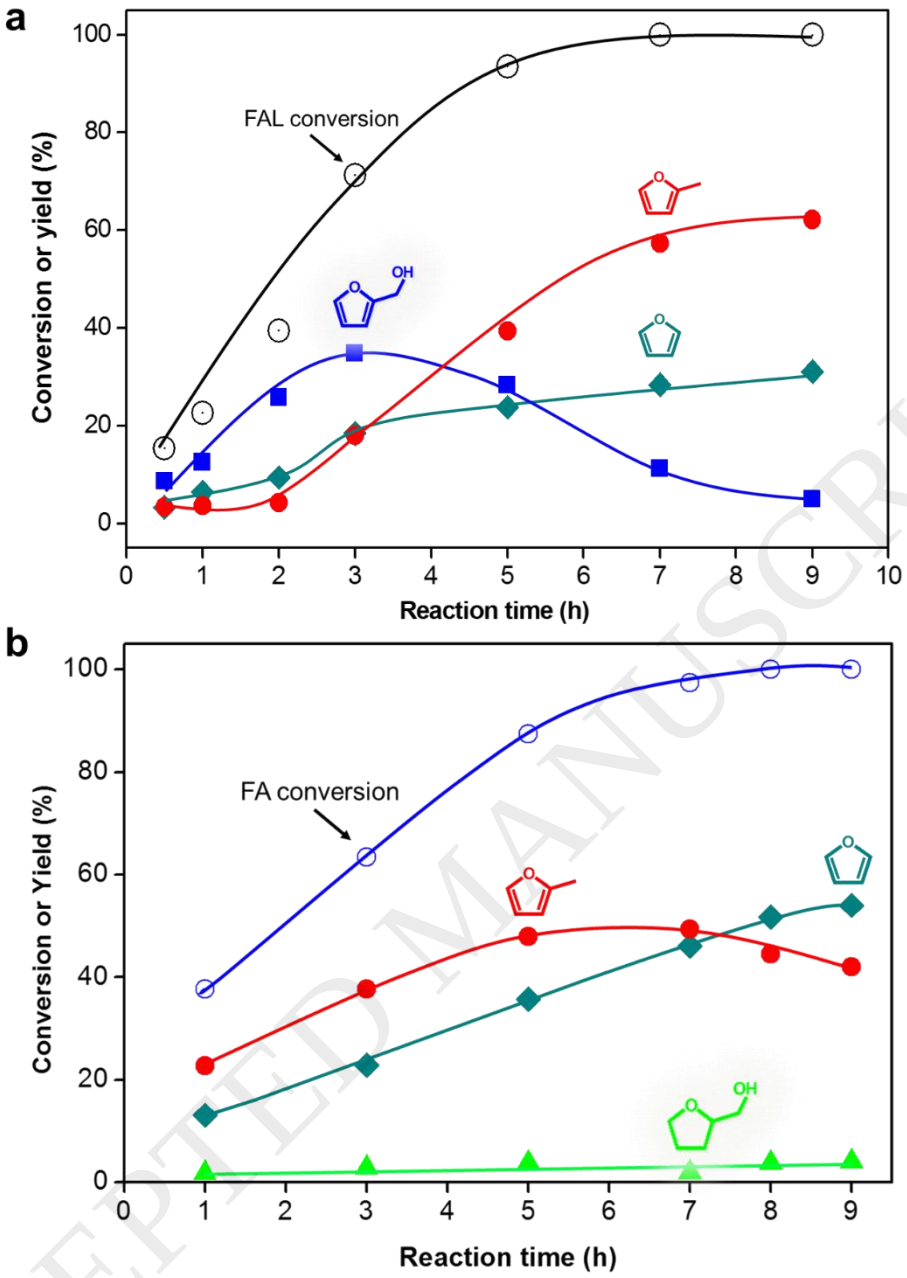

Fig. 8.

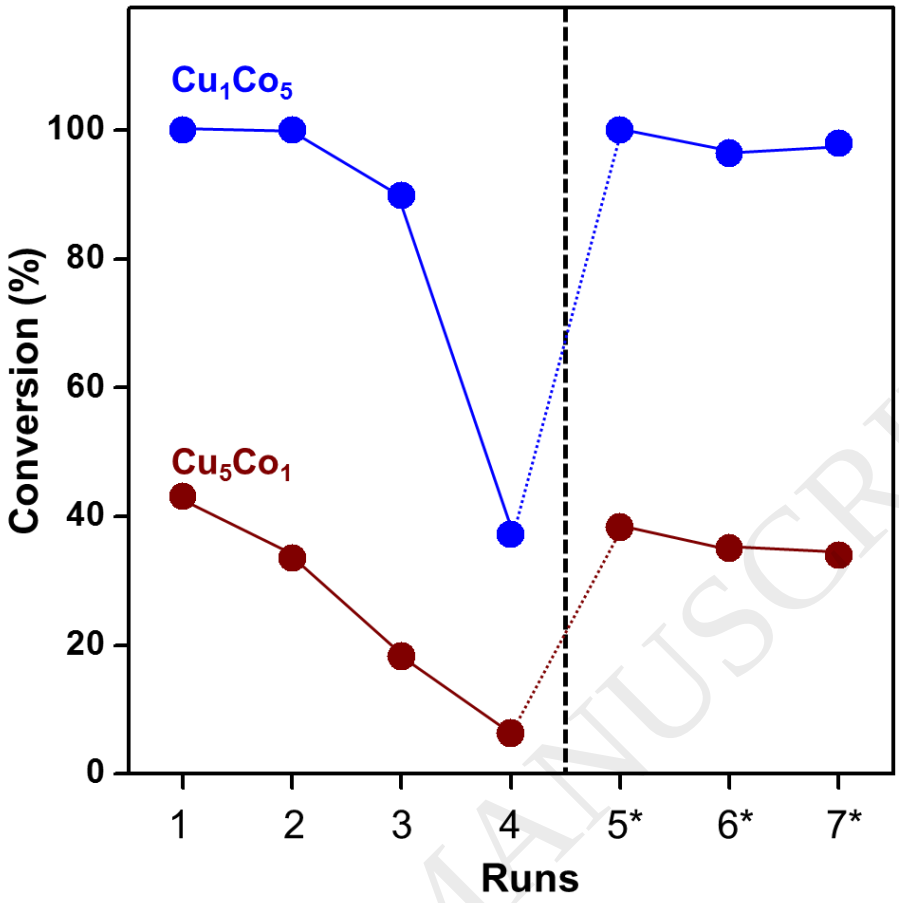

Fig. 9.

List of Schemes

Scheme 1. Schematic illustration of the preparation of mesoporous mixed CuCo oxides: Co in pink and Cu in blue.

Scheme 2. Reaction pathways and corresponding products of the liquid-phase furfural hydrogenation reaction over mesoporous mixed CuCo oxides.

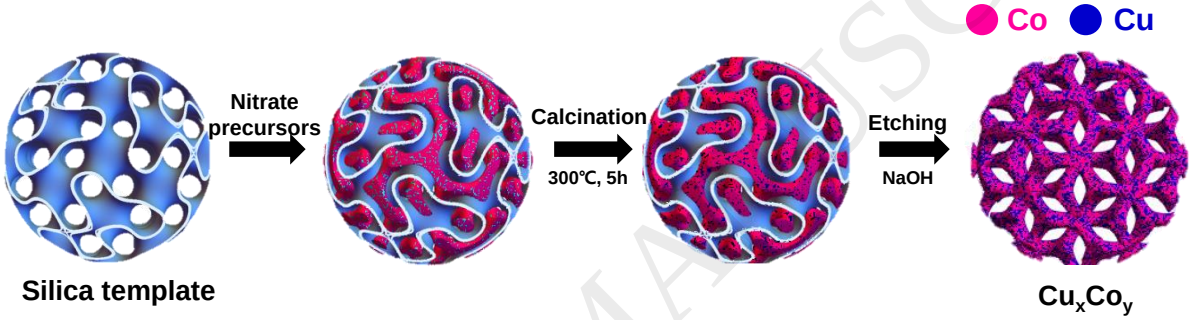

Scheme 1.

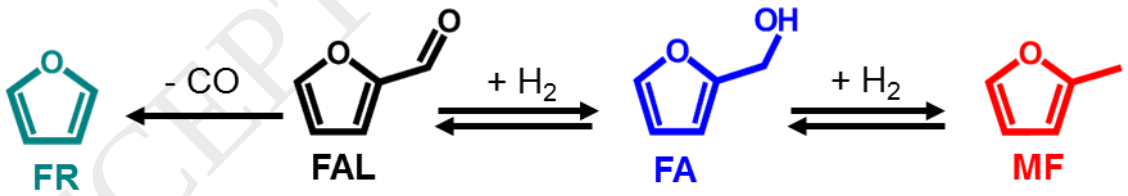

Scheme 2.